

Quantitative evaluation of LAL productivity of colloidal nanomaterials: Which laser pulse width is more productive, ergonomic, and economic?

Alena Nastulyavichus†, Nikita Smirnov, and Sergey Kudryashov

Citation: Chin. Phys. B, 2022, 31 (7): 077803 DOI: 10.1088/1674-1056/ /ac5602
Journal homepage: http://cpb.iphy.ac.cn; http://iopscience.iop.org/cpb

What follows is a list of articles you may be interested in

Strong near-field couplings of anapole modes and formation of higher-order electromagnetic modes in stacked all-dielectric nanodisks

Bin Liu(刘彬), Ma-Long Hu(胡马龙), Yi-Wen Zhang(章艺文), Yue You(游悦), Zhao-Guo Liang(梁钊国), Xiao-Niu Peng(彭小牛), and Zhong-Jian Yang(杨中见)
Chin. Phys. B, 2022, 31 (**5**): 057802. DOI: 10.1088/1674-1056/ac3bac

Improving the performance of a GaAs nanowire photodetector using surface plasmon polaritons

Xiaotian Zhu(朱笑天), Bingheng Meng(孟兵恒), Dengkui Wang(王登魁), Xue Chen(陈雪), Lei Liao(廖蕾), Mingming Jiang(姜明明), and Zhipeng Wei(魏志鹏)
Chin. Phys. B, 2022, 31 (**4**): 047801. DOI: 10.1088/1674-1056/ac1e15

A theoretical study on chemical ordering of 38-atom trimetallic Pd-Ag-Pt nanoalloys

Songül Taran, Ali Kemal Garip, Haydar Arslan
Chin. Phys. B, 2020, 29 (**7**): 077801. DOI: 10.1088/1674-1056/ab99b4

Cascaded plasmonic nanorod antenna for large broadband local electric field enhancement

Dou Zhang(张豆), Zhong-Jian Yang(杨中见), Jun He(何军)
Chin. Phys. B, 2019, 28 (**10**): 107802. DOI: 10.1088/1674-1056/ab3f99

Hot spots enriched plasmonic nanostructure-induced random lasing of quantum dots thin film

Feng Shan(单锋), Xiao-Yang Zhang(张晓阳), Jing-Yuan Wu(吴静远), Tong Zhang(张彤)
Chin. Phys. B, 2018, 27 (**4**): 047804. DOI: 10.1088/1674-1056/27/4/047804

SPECIAL TOPIC — Laser and plasma assisted synthesis of advanced nanoparticles in liquids

Quantitative evaluation of LAL productivity of colloidal nanomaterials: Which laser pulse width is more productive, ergonomic, and economic?

Alena Nastulyavichus[†], Nikita Smirnov, and Sergey Kudryashov

P. N. Lebedev Physical Institute of the Russian Academy of Sciences, Moscow, Russia

(Received 16 November 2021; revised manuscript received 13 February 2022; accepted manuscript online 17 February 2022)

Near-IR (wavelength ≈ 1 μm) laser ablation of bulk, chemically-inert gold in water was compared for different laser pulse width in broad the range of 300 fs–100 ns, comparing a number of key ablation characteristics: mass loss, single-shot crater volume and extinction coefficient of the generated colloidal solutions taken in the spectral ranges of interband transitions and localized plasmon resonance. Comparing to related air-based ablation results, at the given fluences laser ablation in the liquid resulted in the maximum ablation yield per unit energy and maximum NP yield per pulse and per unit energy for the picosecond lasers, occurring at subcritical peak pulse powers for laser self-focusing. The self-focusing effect was demonstrated to yield in incomplete, effectively weaker focusing in the water filaments of ultrashort laser pulses with supercritical peak powers, comparing to linear (geometrical) focusing at sub-critical peak powers. At the other, nanosecond-pulse extreme the high ablation yield per pulse, but low ablation yield per unit energy and low NP yield per pulse and per unit energy were related to strong ablation plasma screening, providing mass removal according to the well-established scaling relationships for plasma. Illustrative comparison of the ablation and nanoparticle generation efficiency versus the broad fs–ns laser pulse width range was enabled in terms of productivity, economicity, and ergonomicity, using the proposed universal quantitative criteria.

Keywords: laser ablation of gold in liquid, ablated mass, critical power for self-focusing, filamentation

PACS: 78.67.Bf, 52.38.Mf, 52.38.Hb **DOI:** 10.1088/1674-1056/ac5602

1. Introduction

Laser ablation in liquids (LAL) is the well-established high-throughput (g/hour) nanofabrication method of colloidal nanoparticles[1–3] and potentially promising, though well-understood yet approach for advanced surface micromachining.[4–6] Different — CW,[7] short-pulse (ns–ms durations)[8–15] and ultrashort-pulse (fs–ps durations)[1,2,8,16–21] were extensively used for colloidal nanoparticle generation, but the optimal, potentially case-dependent pulsewidth range was not identified, despite these numerous efforts.[1–3,7–25] Specifically, absolute possible productivity in mass per time equivalent (in units g/s) and laser-power specific productivity (in units g/J) are of interest, enabling scalability of NP production as a function of laser power, while considering the economic aspects too.[8] The use of a liquid as a medium changes the position of the focus of the laser radiation due to the transition of the air-water interface. So in the works[26,27] the study of the ablation efficiency was carried out depending on the position of the focus relative to the target surface. It was shown in the works that the maximum ablation efficiency was achieved when the focusing of the laser beam was slightly higher than the target surface.

Also, in a number of works, LAL efficiency was investigated as a function of laser pulse repetition rate. It was shown that, at high frequencies, laser radiation is scattered by cavitation bubbles, which leads to a decrease in the efficiency of target ablation. The nanosecond laser generation of gold NPs was investigated in Ref. [27], with the maximum nanoparticle concentration of 0.1 mmol/l and the highest nanoparticle productivity achieved, when the pulse repetition rate was equal to 10 kHz and maximal energy was about 900 μJ. The target geometry and behavior of the cavitation bubble, which has a major influence on the silver NP productivity up to 550 mg/h at *n*-laser ablation, was explored in Ref. [28]. NP productivity of 4 g/h was recently shown for a 500-W ps-laser system that additionally utilized a polygon scanner.[29] Ablation rate of 1.3 g/h was achieved for ablation time of 30 min with Al_2O_3 pressed bulk targets.[1] During one-hour ablation synthesis in a liquid flow setup with a high-power and high repetition rate laser, NPs productivities of up to 4 g/h for gold and platinum could be reached. For picosecond laser pulses the maximum productivity of 8.6 ≈ μg/s was achieved at a pulse energy of 110 μJ and repetition rate of 50 kHz (10 ps, 1064 nm), while the silver nanoparticle productivity, with ps-laser is higher compared to fs-lasers (378-mW laser power, 1-kHz repetition rate, 120 fs).[30] The maximal productivity of 27.5 μg/min was demonstrated for fs-laser generation of Au NPs.[31]

[†]Corresponding author. E-mail: ganuary_moon@mail.ru

© 2022 Chinese Physical Society and IOP Publishing Ltd

Counterintuitively, in many circumstances the increase of laser pulse energy (fluence, intensity), peak or total power may result in corresponding sublinear increase or even diminishing of NP yield, being regulated by intrinsic features of the underlying laser–matter (plume, plasma, *etc.*)[32] or laser–liquid (filamentation, boiling, redeposition) interactions,[33–36] considered below in this article.

Currently, nanosecond LAL is known to proceed via surface phase explosion and plasma formation,[3,8–14] once confining fluid prevents intense surface vaporization during the laser pulse, while liquid vapor bubble emerges on microsecond timescale.[37,38] Dense vapor/droplet plume during threshold-like phase explosion facilitates its optical breakdown and plasma formation,[39] with the resulting opaque ablative plasma regulating the basic parameters of the laser–target interaction[40] — plasma pressure, driving the vapor bubble

$$P_{\mathrm{a}} = 0.6\frac{\Psi^{9/16} I^{3/4}}{A^{1/8}\lambda^{1/4}\tau^{1/8}} \tag{1}$$

in unit Pa, plasma-regulated ablation rate

$$M = 2.66\times 10^{-6}\frac{\Psi^{9/8} I^{1/2}}{A^{1/4}\lambda^{1/2}\tau^{1/4}} \tag{2}$$

in units g/cm^2·s, as a functions of laser intensity I (in units W/cm^2), wavelength λ (in unit cm), and pulse width τ (in unit s), and of material-dependent atomic mass A and average ion charge Z, with the parameter $\Psi = 0.5A\left[Z^2(Z+1)\right]^{-1/3}$.[40] Direct comparison to the literature record results, 1.7 ng/pulse–3 ng/pulse,[8] is in semi-quantitative agreement with the theoretical prediction for the vacuum plasma-mediated ablation of gold, ~ 10 ng/pulse, at the typical values $I \sim 10^9$ W/cm^2, wavelength $\lambda \sim 10^{-4}$ cm, and pulsewidth $\tau \sim 10^{-7}$ s over the 100-micron wide laser focal spot. These highly meaningful scaling relationships established for ns-laser plasma in vacuum and low-pressure buffer gases since 70 s,[40–43] accounting for the finite intensity-dependent size of the ablation spot,[39] were recently justified for LAL conditions in contact ultrasonic studies[32] and NP yield.[11,44–46] However, in this regime there are delayed post-pulse plasma effects,[46–52] dramatically changing the LAL characteristics. Deep local heating and melting of materials underneath the hot ablative plasma by its bremsstrahlung and recombination radiation,[49,51] and pressurization/confining the melt by the expanding plasma (plasma "piston") case, yield in expulsion of micron-scale droplets and total removal up to incredible ≈ 10 μm.[49,52] Surprisingly, these bulk expulsion effect limiting the NP fraction in the ablated products, was observed both in in air[47–52] and liquids.[46] Hence, in the context of sublinear intensity-dependent ablation rate and its transition to melt expulsion at higher intensities, there are obvious intrinsic limitations on NP yield in terms of laser intensity, making favorable upscaling of ablation spot at the fixed optimal laser intensity.

In contrast, in the case of ultrashort-pulse laser ablation, high-fluence (~ 1 J/cm^2) ablation in ambient air occurs more intensively for shorter fs-pulses, than for longer ps-laser pulses,[5,53,54] exhibiting almost one order of magnitude (~ 0.1 μm–1 μm) decrease in the pulsewidth range of 0.1 ps–20 ps. The possible reasons are: (i) nonlinear optical absorption of higher-intensity fs-laser pulses,[55,56] (ii) partial acoustic unloading of the warm dense matter during ps-laser pulses, reducing their expulsive kinetic energy,[57] (iii) deeper laser energy deposition via hot-carrier transport.[5,58] Besides this uncertainty, ultrashort-pulse LAL is affected by laser self-focusing and filamentation in the liquid ambient,[33–35,59] the confinement liquid effect on even shorter material removal step,[60–62] transient bubble formation,[6,36] *etc*. As a result, optimal conditions (fluences, pulsewidths) for ultrashort-pulse LAL were not identified yet, despite a number of focused studies.[1,2,8,15–25] Moreover, there were no so far systematic studies of NP yield in ultrashort-pulse LAL, apparently, because of the many above mentioned incoming circumstances. Furthermore, despite the impressive progress in modeling ultrashort-pulse LAL, there is still intense ongoing theoretical research, involving molecular dynamics[60–62] and molecular hydrodynamics[63] simulations, to catch main features of ultrashort-pulse LAL. Meanwhile, basic qualitative understanding and related quantitative description in ultrashort-pulse LAL are still missing, making necessary novel profound enlightening insights in both experimental studies and theoretical modeling.

More general problem is the absence of universal and economically-justified performance criteria for different laser systems regarding NP productivity, enabling quantitative comparison of their total throughput (*e.g.*, g/s) and power specific productivity (g/W·s) in dry weight form.[8] Similar characteristics are usually considered for ablation performance — rate (depth per pulse, ns/pulse) and ablation efficiency (depth per fluence, cm^3/J).[53,54] However, in many experimental cases drying of colloidal solutions or mass-loss studies for the ablated target are ambiguous because of, *e.g.*, chemical modification (oxidation, adsorption, *etc*.) of colloidal NPs during drying or of ablated products in solutions. Moreover, for up- or down-scaling LAL productivity in different applications physicochemical intensive (mass specific — concentration, optical density, *etc*.), rather than extensive characteristics would be more convenient for fast evaluation of productivity, for efficient development and harnessing of LAL technology.

In this study, comparative studies of short- and ultrashort-pulse near-IR LAL of bulk and thin-film samples of chemically-inert gold in water were performed in terms of ab-

lated mass and NP yield versus laser energy, pulse width, and exposure per spot. These studies were focused to identify optimal laser parameters for maximal total NP yield and its power specific throughput, using the product of spectrally-dependent extinction coefficient of colloidal solutions and their volume as a convenient productivity parameter, characterizing both ablated mass and NP yield.

2. Experimental setup and details

In this experiment, a fiber laser Satsuma (amplitude systems, central wavelength 1030 nm, pulse energy $E = 0$ μJ–10 μJ, repetition rate $f = 0$MHz–2 MHz) was used for laser ablation of gold (in purity 99.99%) plate. The full-width at the half-maximum (FWHM) duration of the ultrashort laser pulses was varied via their chirping by an output compressor in the interval $\tau_L = 0.3$ ps–10 ps and measured by a scanning interferometric autocorrelator AA-20DD (Avesta Project). The 1030-nm laser pulse energy in the TEM_{00} mode was smoothly varied, using a thin-film reflective attenuator. The laser pulses were focused onto the sample surface through a microscope objective (numerical aperture NA = 0.65) into a spot with a 1/*e*-radius $\sigma_{1/e} \approx 1$ μm (peak fluence range ≈8 J/cm^2–64 J/cm^2). The single-shot laser ablation of fresh spots of a polished plate of gold was performed in ambient air and distilled water, where the thickness of the liquid layer above the sample surface was ≈ 1 mm. The gold sample was arranged on a three-dimensional motorized stage and moved in 10-micron steps from the shot to shot until the production of 5 craters per each incident pulse energy for each laser pulsewidth and environment. Energy was measured as it exited the lens. Reflection from the water surface was not taken into account. The topology of the ablated surfaces was visualized, using a scanning electron microscope (SEM) JEOL 7001F (JEOL). The profiles of the resulting craters were characterized in a contact mode by a scanning probe microscope (Certus Standard V). The AFM scanning lateral resolution is ≈ 80 nm.

For nanoparticles generation by method of laser ablation in liquid are used: fiber laser Satsuma and nanosecond Yb-doped fiber laser HTF MARK (Bulat) ($\lambda = 1064$ nm, FWHM pulse width of 100 ns, maximum pulse energy $E_{max} = 1$ mJ, and pulse repetition rate $f \leq 80$ kHz. The laser beam was focused by a galvanoscanner with an objective focal length ≈ 100 mm onto Au target placed on the bottom of a cuvette and immersed in 3 ml of deionized water (height above the target ≈ 1 mm). Several ablation regimes with different effective number of pulses at the point $N = 0.5$–80 pulses and pulse energy ($E = 2.5$μJ–6.5 μJ for fs/ps-laser pulses, $f = 20$ kHz, and 0.3 mJ–0.6 mJ for ns-laser pulses, $f = 20$ kHz) were investigated. Pulse repetition rate was fixed and equal to 20 kHz. The minimum size of the focusing spot (1/*e*-diameter) $2\sigma_{1/e} \approx 20$ μm for fs/ps-laser pulses and ≈ 50 μm for ns-laser pulses. The size of the scanning area was 10 mm × 20 *mm*.

Transmission spectra of the colloidal solutions were recorded by means of a UV-IR spectrometer (SF-2000, OKB Spectr) in the range of 190nm–1100 nm. Scanning electron microscopy (SEM) visualization of the produced nanoparticles was performed using a JEOL 7001F microscope (JEOL, Japan), equipped by an energy-dispersion x-ray spectroscopy (EDX) module INCA (Oxford Instruments, England) (Oxford Instruments) for chemical microanalysis of Au nanoparticles at 10-keV kinetic electron energy. Nanoparticle size distributions were analyzed by means of a dynamic light scattering analyzer Photocor Compact. Weight loss was measured using a microbalance AND BM-20. The experimental setup is shown in Fig. 1.

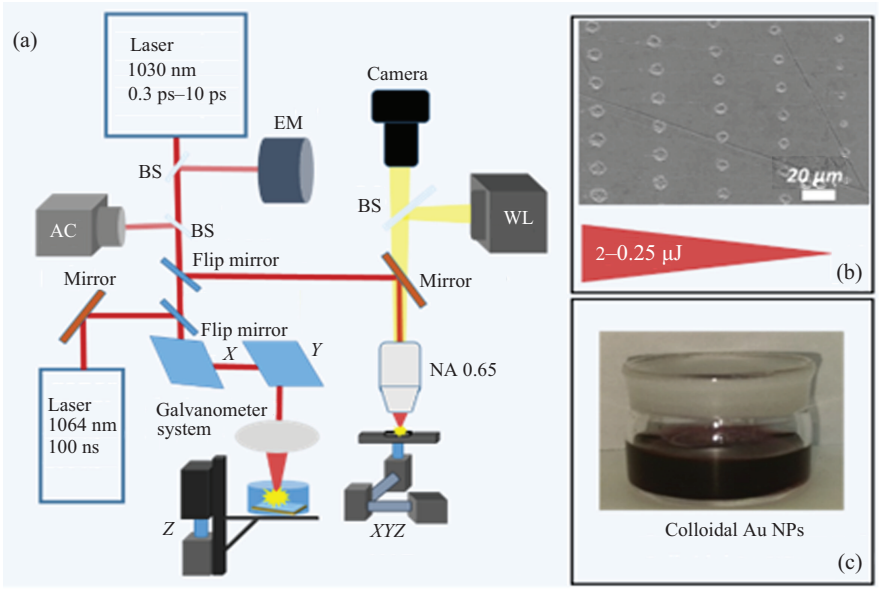


Fig. 1. (a) Layout of experimental setup for single-shot high-NA ablation in air and water, and multi-shot low-NA LAL in water. (b) Top-view SEM image of single-shot crater son the gold surface. (c) Colloidal NPs of gold in water.

3. Experimental results

3.1. Record Au-LAL: single-shot fs- and ps-LAL efficiency

Our methodological research was started from 0.3- and 10-ps single-shot LAL of bulk gold in water *versus* laser fluence (Fig. 2). For more consistent analysis, we compare fluence dependences not for the single-shot (SS) crater depths (ablation rates) (Fig. 2(b)), but for the corresponding ablated (removed) volume V_S (Fig. 2(a)). This approach allows accounting for potential beam distortions due to self-focusing and filamentation in water, and lateral melt expulsion at high-NA focusing, also affected by the water confinement.

The employed fluence range and typical smooth submicron-deep, melt-flow decorated crater topographies indicate the supercritical "phase-explosion" (PE) regime,[58] providing efficient fluence-dependent increase of ablated mass as compared to fluence-independent shallow "spallative" ablation $\sim$ 10 nm/pulse–20 nm/pulse.[59] This is strongly contrasting to shallow spallative craters, decorated for the reason of weak mass removal by laser-induced periodical surface structures in Ref. [8] (similarly in Ref. [23]), where the maximal ablated mass $m_{spal} \approx 320$ pg/pulse was achieved, being a record value to the date.

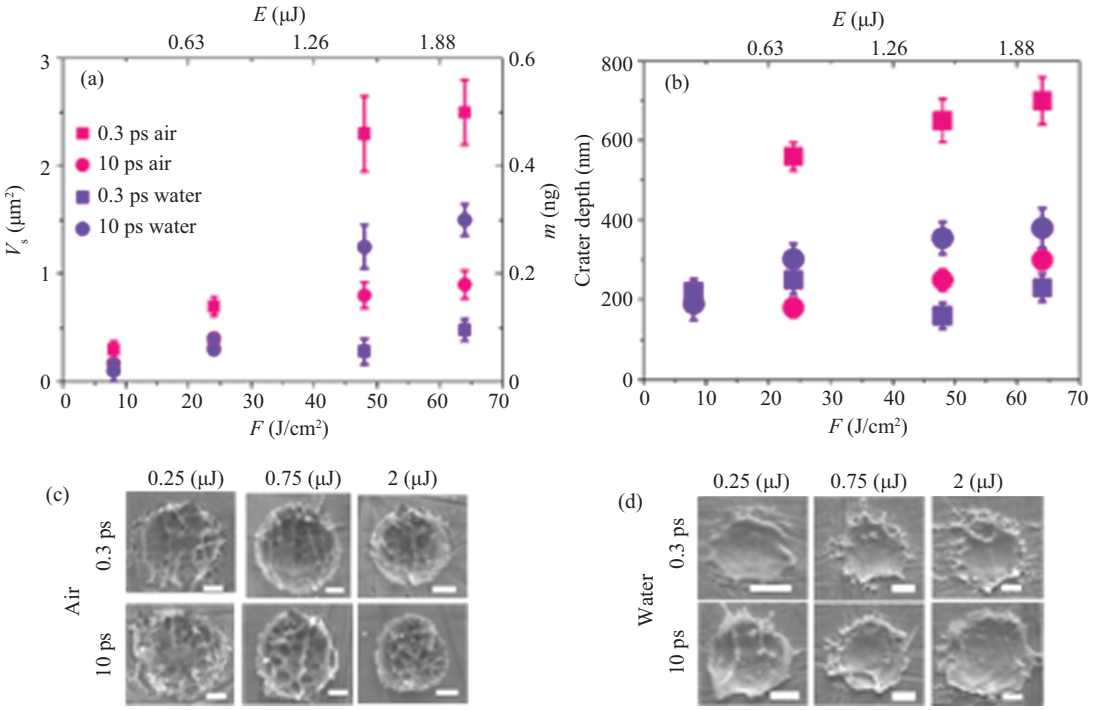


Fig. 2. SS-ablated volume/mass (a) and maximal-ablated depth (b) *versus* laser fluence (energy) at 0.3–ps pulsewidths and 10-ps pulsewidths and different ambient media: air (pink symbols) and water (violet symbols). Left and right columns: Top-view SEM images of SS craters for air (c) and water (d). Scale bar: 1 μm.

In Fig. 2 for the SS air-based ultrashort-pulse laser ablation one can find the common monotonic increase of the ablated volume versus laser fluence in the PE regime,[64] but simultaneous two- or three-fold decrease versus the increasing pulsewidth (0.3 ps–10 ps) at comparable fluences. Particularly, the ablated volume magnitude starts to decrease explicitly for $\tau > 1$ ps (Fig. 3(a)) by 2–3 times, being more pronounced at higher pulse energies (fluences), representing the phase explosion, rather than fluence- and pulsewidth-independent spallation regime.[5,65] This is consistent with previous studies for other materials (*e.g.*, copper[66]). There are a few plausible explanations of the pulsewidth-dependent downcoming trend, related to (i) stronger nonlinear absorption in transition metals at higher laser intensities provided by shorter pulses,[55,56], (ii) ultrafast hot-carrier transport during shorter pulses until electron-lattice thermalization[5,52], and (iii) partial unloading of GPa-level internal pressure during longer pulses, reducing expulsion of supercritical fluid.[57] Surprisingly, during our SS wet ablation in water (LAL) the ablated volume increases for longer pulses at comparable laser fluences (Figs. 2 and 3), the trend, previously also observed for silicon.[5]

Specifically, for the SS LAL of gold in water the ablated volume and mass changes similarly to the air-based ablation at lower pulse energies (fluences) < 1.6μJ (Fig. 3(b)), while considerably increases at the intermediate pulsewidths of 1 ps–7 ps at higher pulse energies, finally slightly decreasing for longer pulses. Comparing to the maximal ablated mass $m_{spal} \sim 320$ pg/pulse per 1030-nm, 97-μJ, 3-ps pulse reported in for shallow, spallative ablation,[8] the observed SS ablated mass $m_{pe} \approx 60$ pg/pulse per 1030-nm, 2-μJ, 4-ps pulse in Fig. 3(b) appears five-fold lower. However, in the ergonomic (energetic) sense, ablation efficiency (energy-specific ablated mass, m/E) ~ 20 μg/J (pg/μJ) in Fig. 3(d) (4-ps, 1030-nm pulses) by one order of magnitude exceeds that one ~ 3 μg/J (3-ps, 1030-nm pulses) in Ref. [8].

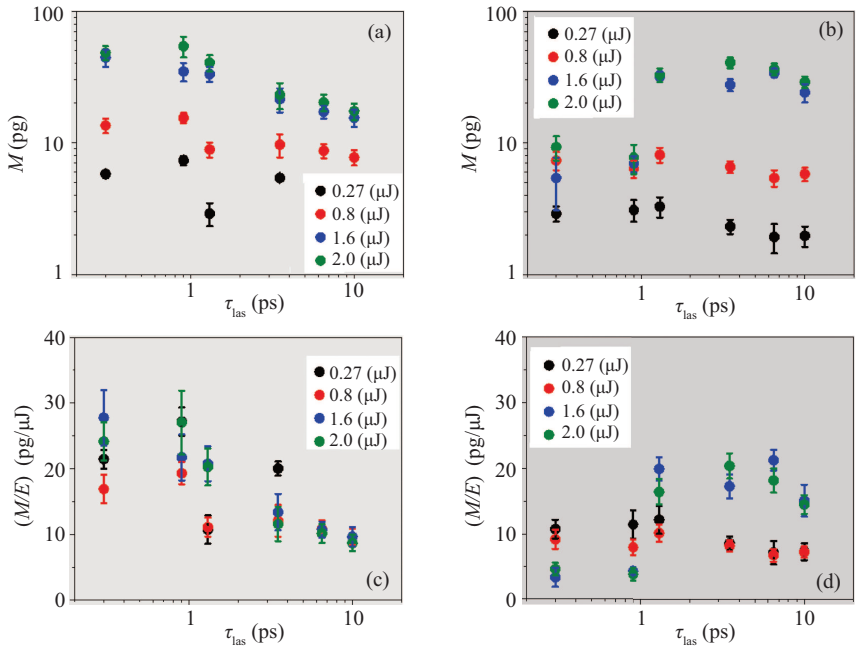


Fig. 3. Pulsewidth dependences at different pulse energies for SS-ablated mass (panels (a) and (b)) and energy-specific SS-ablated mass (panels (c) and (d)) in air (panels (a) and (c)) and water (panels (b) and (d)).

3.2. Realistic Au-LAL: Multi-shot fs-, ps-, and ns-LAL efficiency

In real mass-production multi-shot (MS), raster-scanning LAL regimes, one cannot avoid vibration, displacement, and energy instabilities in managing precisely focusing and other auxiliary effects, like in single-shot experiments (Figs. 2 and 3), with both ablation productivity and ablation efficiency (energy-specific ablation productivity) becoming generally lower. This is exactly what we observe for MS (exposure $N \sim$ 1–10 shots/spot) scanning-mode LAL, producing the overall sample mass loss ΔM and colloidal nanoparticles in water. Owing to the rather inert (non-oxidizing at normal ambient conditions) character of gold, the overall mass loss normalized to the gold density $\rho_{Au} \approx 20$ g/cm^3 and the overall number of shots to provide the ablated volume $V_M = (\Delta M/\rho)N$ (Fig. 4(a)), could be directly compared to V_S and ablated mass per pulse in Fig. 3(b).

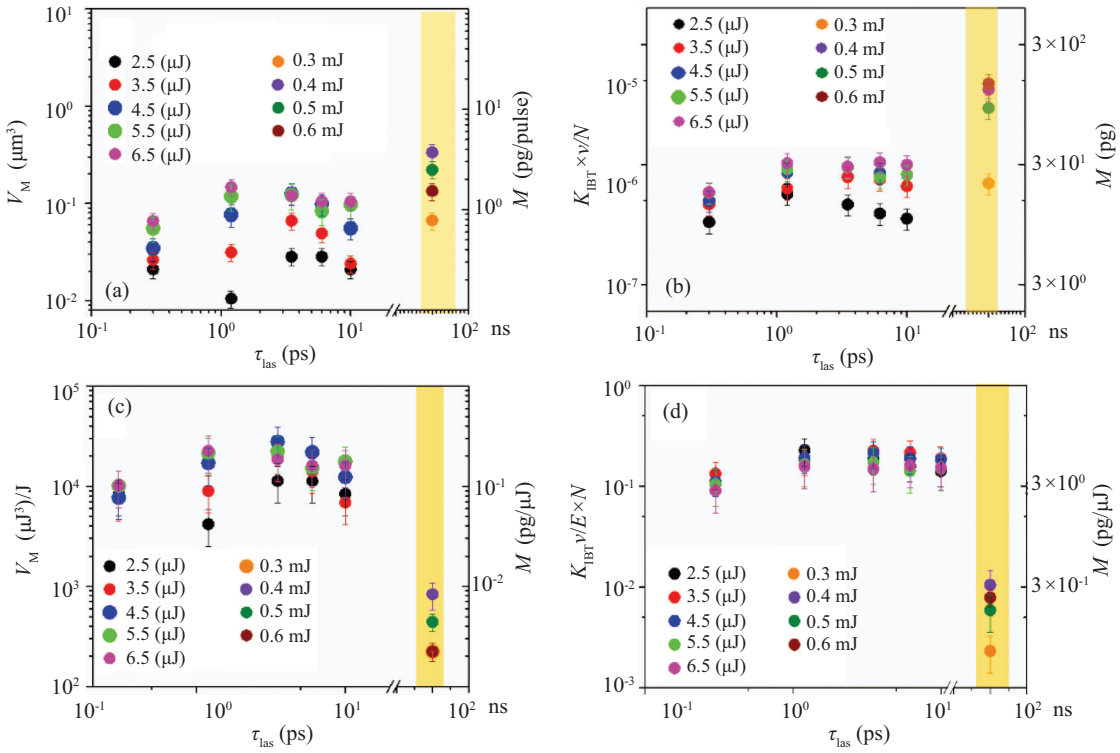


Fig. 4. Pulsewidth dependences at different pulse energies for (a) MS-ablated volume V_M and mass per pulse in water ($N = 10$); (b) normalized extinction coefficient $\kappa_{IBT} \times \nu/N$, and MS-ablated mass m_{coll} in the volume ν per pulse during LAL in water; (c) and (d) their energy-specific values.

In this work, for the same pulse energy, though at different – 0.65-NA (SS) and 0.05-NA (MS) — focusing, one can see the one order of magnitude higher ablation yield in the high-NA SS-regime (Fig. 3(b)), comparing to 0.05-NA MS-ablation (Fig. 4(a)). Specifically, the maximal value of 60 pg/pulse for 4-ps, 0.65-NA SS LAL (Fig. 3(b)) is much higher, than 3 pg/pulse for 1-ps, 0.05-NA MS LAL (Fig. 4(a)), while keeping the same PE LAL regime (Fig. 5). Here, one can guess that potentially higher fluence (with the weaker filamentation effects at lower peak powers) in the former case supports more efficient removal in the confining medium, as supposed in Ref. [60]. Moreover, transient absorbing NP-colloid[11] and/or scattering vapor-bubble[2,67] screening effects in the MS-LAL scanning mode could also reduce the laser-surface coupling and ablation, besides possible secondary re-deposition effect.[36] Importantly, ns-LAL demonstrates a few times higher MS-ablated volume and ablated mass in Fig. 4(a), provided in the plasma-mediated regime at the two-orders of magnitude higher incident pulse energies.

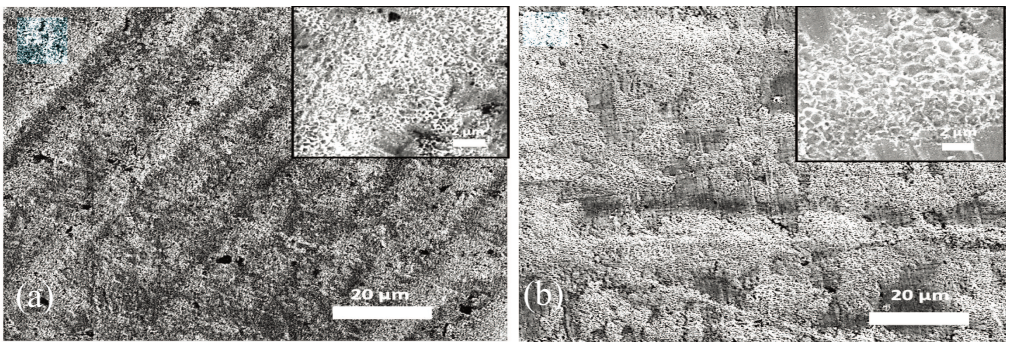


Fig. 5. SEM images of micron-deep surface relief produced by MS fs- (a) and ps-laser (b) gold ablation.

The observed correlation between the ablation characteristics V_S, V_M, and NP generation parameter $\kappa_{IBT}\nu/N$ in Figs. 3 and 4 provides a unique facile opportunity to envision ultrashort-pulse LAL of gold in water from the different sides and to obtain enlightening insights in still poorly unveiled LAL processes – removal in spallation and phase explosion regimes, redeposition, cumulative optical and hydrodynamic effects during LAL, dispersion/sedimentation of ablation products in water.

Above we demonstrated that extinction coefficients of colloidal gold solutions correlate well with other basic ablation characteristics, such as, for example, single-shot or multi-shot ablated volume (Figs. 2–4). Here, we use the extensive parameter "extinction volume" (EV)- product of the extinction coefficient κ of Au–NP colloidal solutions and the solution volume ν, $\kappa \times \nu$ [in unit cm^2], to characterize and compare absolute productivity of colloidal gold solutions for different laser systems and ablation regimes per the extensive parameter of pulse energy, both in terms of gold content (EV value $\kappa_{IBT} \times \nu$, ablated mass per pulse $m_{coll} = \{\rho_{Au} \times \nu\} \times \{\kappa_{IBT}/\kappa_{IBT,0}\}/N$, where $\kappa_{IBT,0} \approx 6 \times 10^5$ cm^{-1} is the absorption coefficient of bulk gold at 400 nm[68] and its dispersion in the solutions ($\kappa_{LPR} \times \nu$). Below, in Fig. 6 we use EV to compare systematically, for the first time, gold NP generation by fs-, ps-, and ns-laser pulses.

The corresponding EV values measured at quite similar focusing conditions, but for different 1-μm laser fluences, repetition rates and scanning speeds typical for these laser systems, enable their facile comparison in terms of "colloidal" ablated mass m_{coll} and colloidal ablation efficiency m_{coll}/E (Fig. 6). Specifically, indicate the rapid decrease vs laser exposure for $N > 1$ (Figs. 6(a)–6(c)), consistent with our and other previous observations.[2,10,16,67] Surprisingly, in the case of fs-LAL despite the high starting EV values $\sim 10^{-4}$ cm^2, the cumulative N-dependent decrease occurs no-linearly as $1/N^2$ (Fig. 6(a)), while in the ps-LAL and ns-LAL regimes the cumulative decrease from the starting EV magnitudes $\sim 10^{-5}$ cm^2 varies as $1/N$ (Fig. 6(b)) or even slower (Fig. 6(c)), respectively. Meanwhile, in all these case the strong pulse-energy dependence of EV implies the potential EV scalability in terms of total laser energy accumulated during the sample ablation at the same exposure per spot (no spatial cumulative effects) and the obvious necessity of flow reactors for NP- generation with continuously refreshing wire-like or band-like ablation target, as it is currently used in the advanced reactors.[69,70]

In this context, for more correct comparison of ablation and NP generation efficiencies provided by the different laser systems we also derived energy-specific volume extinction $\kappa_{IBT} \times \nu/(E \times N)$, resembling power-specific productivity in Ref. [8] or power-specific ablation rate in general. In relation to this parameter, in the given exposure range $N = 1$–100 the employed near-IR ultrashort-pulse laser (pulsewidths ≈ 0.3 ps–10 ps) and short-pulse laser (pulsewidth ≈ 100 ns) demonstrate the more advantageous ultrashort-pulse LAL with $\sim 10^{-4}$ cm^2/J–0.1 cm^2/J (Figs. 6(d) and 6(e)), which is more than order of magnitude more efficient per unit energy, comparing to ns-LAL (Fig. 6(f)).

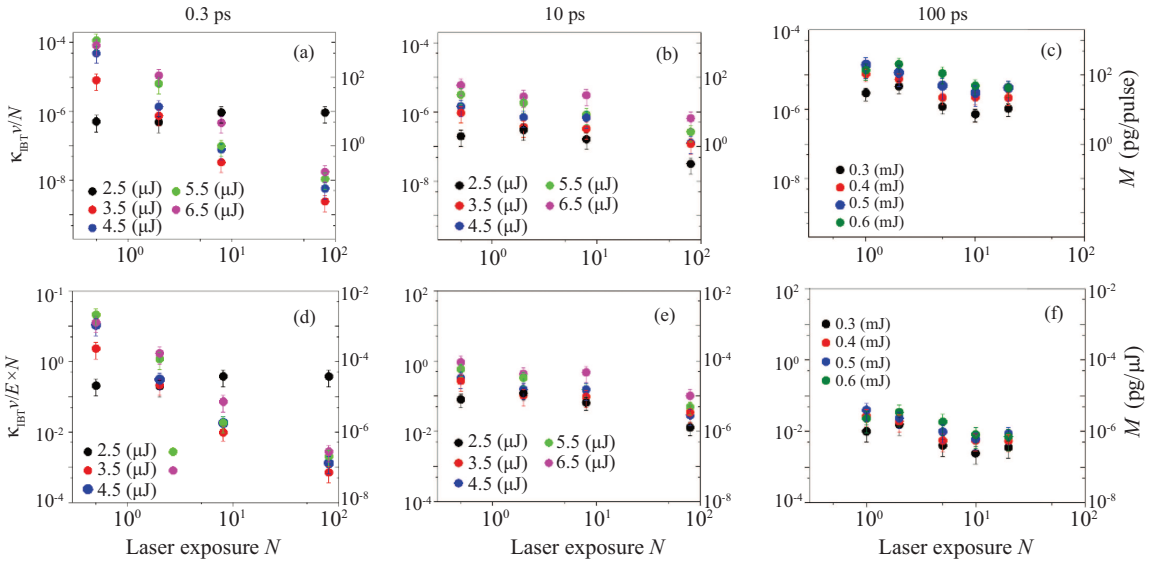


Fig. 6. (a)–(c) Exposure dependences of extinction volume per pulse $\kappa_{IBT}v/N$ (cm^2/pulse)/colloidal ablated mass m_{coll} (pg/pulse), and (d)–(f) energy-specific EV $\kappa_{IBT}v$/(EN) (cm^2/J)/colloidal ablation efficiency m_{coll}/E (μg/J) for gold-NP colloidal solutions at different pulsewidths and energies.

Furthermore, using the EV characteristic of ablated mass in the gold NP solutions of the same volume v, we considered a normalized extinction coefficient $\kappa_{LPR}/\kappa_{IBT}$ to evaluate dispersion of the material, where the higher ratio value indicates the higher dispersion of the same mass over NPs in different ablation regimes and for different laser systems (Fig. 7). One can find higher dispersion $\kappa_{LPR}/\kappa_{IBT}$ ≈1–4, in the case of fs-LAL (Fig. 7(a)), while ps-LAL and ns-LAL exhibit much lower dispersion (Figs. 7(b) and 7(c)). In the ps-LAL regime such effect could indicate expulsion of larger particles, while in the case of ns-LAL one can expect expulsion of even micro-droplets,[46] apart from the accompanying small-size plasma-mediated dissociation/recondensation products.[71]

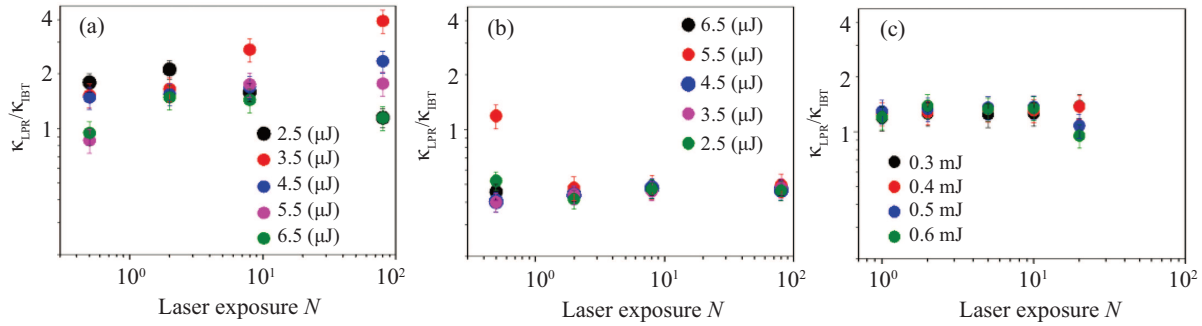


Fig. 7. Normalized extinction coefficient $\kappa_{LPR}/\kappa_{IBT}$ of Au–NP colloidal solutions in LPR *versus* laser exposure at the different pulsewidths: 0.3 ps (a), 10 ps (b), and 100 ns (c).

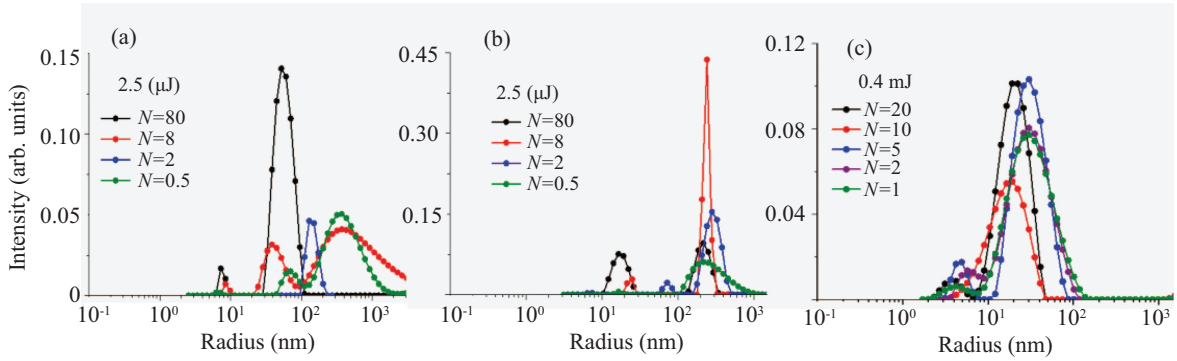


Fig. 8. DLS spectra of gold NPs at the different laser exposures and pulsewidths: 0.3 ps (a), 10 ps (b), and 100 ns (c).

Indeed, our DLS analyses demonstrated both nanoscale (10 nm–100 nm) and sub-micron (100 nm–1000 nm) particles in the fs-LAL regime (Fig. 8(a)), while mostly sub-micron particles (100 nm–1000 nm) were predominating in the ps-LAL regime (Fig. 8(b)), in contrast with ultra-small (10 nm–100 nm) particles formed through dissociation/recondensation

in ns-LAL plumes (Fig. 8(c)). The observed NP abundances consistently represent the known general ablation features of these LAL regimes.[8–14,44–46] In addition, for the 0.3-ps duration a narrow distribution is observed within 70 nm–100 nm; there are no changes with the increasing energy, as in the case of ns-laser ablation. For the 10-ps pulse duration, the distribution is wide and the particle size varies from 20 nm to 500 nm. With an increase in energy, a decrease in particle size is observed. With increasing pulse duration for fs-ps laser ablation, a slight increase in particle size is observed, but for ns-laser ablation, in general, particle sizes are smaller. As the scan speed increases, there is an increase in sizes for all pulse durations.

3.3. How the fs/ps-width affects the LAL efficiency?

Above we qualitatively mentioned the downcoming peak pulse power-dependent trend in LAL regarding the ablated volume and IBT-related extinction coefficient of the resulting colloidal solutions. Specifically, one can find that the most significant and highly nonlinear increase of these quantities occur at peak pulse powers (Fig. 9), well below the known critical power for self-focusing in water at the 1030-nm wavelength, $P_{cr} \approx 1.5$ MW,[5,23,27,28], *i.e.*, mostly as fluence (peak intensity) dependences of the ablation parameters. Furthermore, this potentially indicates the onset of filamentation and its influence on the ablation (Figs. 9(a) and 9(b)) and NP generation in water (see Fig. 9(c)) at supercritical-power propagation conditions. Indeed, in contrast at supercritical peak powers, achieved in this work for 0.3-ps laser pulses, both the ablated volume (see Figs. 9(a) and Fig. 9(b)) and the NP yield (see Fig. 9(c)) demonstrate either saturation, or much slower increase *versus* P.

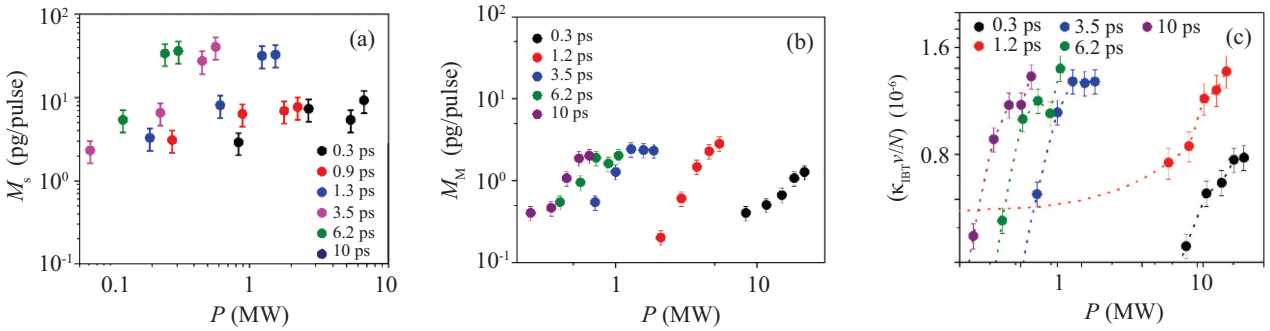


Fig. 9. Peak pulse power dependences of single-shot (a) and multi-shot (b) ablated volume per pulse, and (c) extinction coefficient in the volume v per pulse $\kappa_{IBT} \times v/N$ during water-based LAL.

In this context, we performed transverse Y,Z-scan profiling of local beam size in the focal region of 0.3- and 10-ps laser pulses in water, using a 30-nm thick gold film as a photosensitive target for tracking of ablation spots (Figs. 10(a) and 10(b)). The precise focal positions could be identified as minimal circles (Fig. 10(b)), free from the astigmatic aberration, making beam more extended in the x direction prior focus and in the y direction after the focus.[72] For the reason of the non-circular (elliptical) shapes of the ablation spot prior and beyond the focus, we chose, as a quantitative focusing characteristic, the through hole square — the product of ellipse radii a and b, $S = \pi \times a \times b$, with its minimum at the focal point during geometrical focusing (Figs. 10(c)–10(e)). For the Gaussian fluence distribution

$$F(r,z) = \frac{E}{\pi\sigma_{1/e}^2(z)} \exp\left(-\frac{r^2}{\sigma_{1/e}^2(z)}\right) \tag{3}$$

with the local beam radius $\sigma_{1/e}(z)$

$$\sigma_{1/e}^2(z) = \sigma_{1/e}^2(0)\left(1 + \frac{\lambda^2 z^2}{\pi^2 n^2 \sigma_{1/e}^4(0)}\right), \tag{4}$$

one can directly relate the size of the ablated spots with the local with the radius $\sigma_{1/e}(z)$ at the arbitrary point z as

$$\begin{aligned} R_{abl}^2(z) &= \sigma_{1/e}^2(z)\left(\ln E - \ln[\pi\sigma_{1/e}^2(z)F_{abl}]\right) \\ &\propto \sigma_{1/e}^2(z)[\ln E - C]. \end{aligned} \tag{5}$$

The corresponding squares in Figs. 10(c)–10(e) reasonably represent the squared characteristic $1/e$-intensity radius $\sigma_{1/e}$, *i.e.*, for the fixed pulse energy and the constant ablation threshold ($R_{abl}(z) \gg$ heat diffusion length) — near-waist focusing in water.

Experimentally, at the several incident pulse energies for the 0.3-ps and 10-ps pulses and focusing with an objective focal length ≈ 100 mm for ns-laser pulses we observed the geometrical focusing for the longer pulses (Figs. 10(c)–10(e)) and the onset of nonlinear focusing (self-focusing) and filamentation for the shorter pulses, with the clamped above-threshold beam square in the filaments. Specifically, for the supercritical 0.3-ps laser pulses at all these pulse energies one can observe the onset of the nonlinear focus at $z \approx -500$ μm, with the accompanying expected clamping[59,73] of the ablated spot (laser beam?) square at the level, twice higher than the minimal one in the geometrical focal point. However, near the

geometrical focal point there are global minima of the ablated spot square for the 0.3-ps laser pulses, approaching almost the same minimal values, as for the linear focus of the 10-ps laser pulses (Figs. 10(c)–10(e)). These novel findings indicate that despite the proceeding self-focusing of the super-critical 0.3-ps laser pulses in water (mostly, in its central intense part), their minimal focal size is still dictated by the external focusing power,[74,75] apparently, for the low-intensity laser beam periphery. In any case, the maximal laser intensity (fluence) in the focal region for the supercritical peak laser powers appears to be considerably lower, resulting in much weaker ablation and NP generation (Fig. 9).

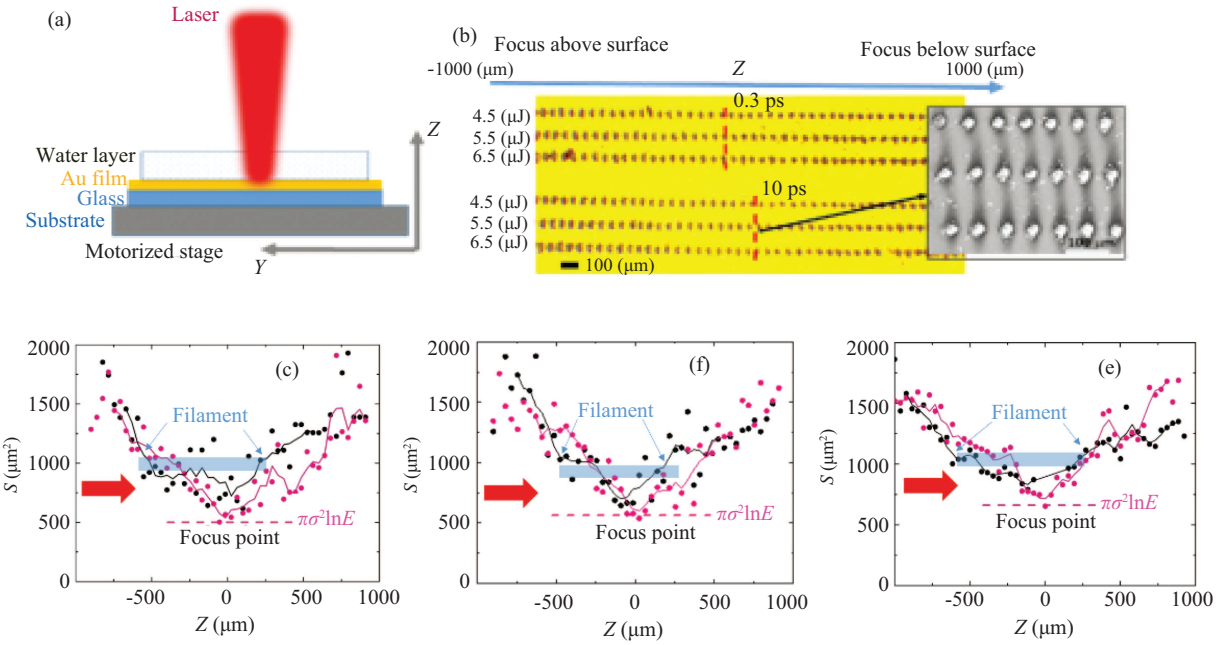


Fig. 10. (a) Layout of Y, Z-scanning measurements of squares of water-based ablated spots in the 30-nm gold film. (b) Optical images of the Y, Z-scanned gold film (inset-SEM image of focal position). (c)–(e) Z-dependences of S at the 4.5- (c), 5.5- (d), and 6.5- (e) μJ energies of 0.3- (dark circles) and 10-ps (red circles) pulses, and their smoothed curves of the corresponding colors, showing the zero (focal position), the expected beam square $\pi\sigma_{1/e}^2 \ln E$, and filament length/position shown by the blue rectangle. The red arrows show the laser beam propagation direction.

3.4. Discussion

Our current and previously reported experiments[44–46] indicate that at the above-threshold conditions plasma-mediated ns-LAL exhibits the almost linear yield vs intensity I (the product of the square-root intensity dependence of ablation rate corrected for the above-threshold ablation spot). This fact enables focal/ablation spot-upscaling vs pulse energy E at the fixed above-threshold intensity, once energy-dependent vapor-bubble dimensions are neglected in terms of surface screening. Meanwhile, in this study we demonstrate that ns-LAL dramatically gives up regarding energy-specific ablation and NP-generation efficiencies (Figs. 6(d)–6(f)) because of parasitic plasma screening, typical for ns-laser ablation. Simultaneously, the ns-laser intensity range, where ns-LAL could proceed via phase explosion without plasma screening, is rather narrow (*e.g.*, ≤ 0.1 GW/cm^2 above the phase explosion threshold[39]). Moreover, at the above-threshold ns-laser intensities NP yield saturates because of the accompanying microdroplet expulsion (unfavorable for NP generation), both in air[47–52] and in solutions.[16,46]

In contrast, in the case of gold targets ps-LAL in the phase explosion regime appears to be most efficient and pulse-energy scalable, being almost as efficient, as air-based fs-laser ablation, while fs-LAL considerably suffers from self-focusing and filamentation in water (Figs. 9(b) and 9(c)), occurring at the 1030-nm laser wavelength for peak pulse powers, exceeding 1 MW–2 MW[5,23,27,28] (sub-μJ pulse energies for sub-ps laser pulses). Moreover, even in these regimes the ablation efficiency and NP productivity upscaling becomes possible at higher pulse energies and multi-critical peak pulse powers, if advanced temporal[73,76,77] or spatiotemporal[78–81] focusing arrangements are employed. The first approach utilizes linear focusing of pre-chirped picosecond laser pulses with sub-critical pulse powers, becoming compressed in the focal region upon their propagation in a liquid with normal dispersion, once were initially negatively pre-chirped.[64] The second, more sophisticated approach is based on spatio-spectral transformation of ultrashort laser pulses.[81] Specifically, the spectral components of the incident ultrashort laser pulse are spatially separated, resulting in a rainbow-like collimated beam, while spatially reducing the local bandwidth and increasing the pulse duration. Downstream from the focusing optics, the previously separated spectral components start to overlap, with the gradual recovery of the entire bandwidth and initial ultrashort

pulse duration within the focal volume. In addition to the minimization of nonlinear effects, the intensity in front of the focus is reduced owing not only to the geometrical change of the beam diameter but also to the change of the pulse duration. Consequently, the nonlinear laser–material interaction is more strongly confined to the focal volume than for conventional focusing.[81]

Regarding NP generation during LAL, direct comparison of ablation efficiency and NP productivity for different laser systems and experimental conditions becomes conveniently possible, utilizing the informative criteria of "extinction volume" per pulse (EV, $\kappa \times v/N$ [in unit cm^2]) or "colloidal" ablated mass ($m_{\rm coll} = \{\rho_{\rm Au} \times v\} \times \{\kappa_{\rm IBT}/\kappa_{\rm IBT,0}\}/N$, [in unit g]) (Figs. 6 and 9), and energy-specific extinction volume per pulse ($\kappa_{\rm IBT} \times v/(E \times N)$ [in units cm^2/J]) or "colloidal" ablation efficiency ($m_{\rm coll}/E$, [in units g/J]), proposed in this study. Similarly to NP-generation productivity,[8,16] the EV values acquired in the interband-transition spectral range, characterize the amount of suspended ablated matter in the given solution volume, while similar parameter acquired in the localized plasmon resonance of gold nanoparticles, shows the ablated material dispersion over different nanoparticles. DLS analyses demonstrated both nanoscale (10 nm–100 nm) and sub-micron (100 nm–1000 nm) particles in the fs-LAL regime, while mostly sub-micron particles (100 nm–1000 nm) were predominating in the ps-LAL regime, in contrast with ultra-small (10 nm–100 nm) particles formed through dissociation/recondensation in ns-LAL plumes. Given per pulse, extensive EV values can be upscaled by increasing extensive parameter of pulse energy in high-power pulsed lasers, still more readily feasible for ns-lasers. However, as energy-specific EV gives a clue of ergonomic and operational costs during LAL and NP generation by the given laser system, alike to power-specific productivity in Ref. [8], ps-LAL, alike to air-based fs-laser ablation, exhibit the highest productivity in terms of this quantity in NP production at high (multi-MHz) pulse repetition rates,[82,83] scalable vs pulse energy (Figs. 9(b) and 9(c)). Still, more comprehensive analysis could include other evaluation factors.[84] To note, even though in our study we have intentionally limited ourself by near-IR laser pulses of the different durations, in general, similar studies could be extended to other laser wavelengths and pulse durations (till CW).

4. Conclusion

In this study, near-IR (wavelength ≈ 1 μm) laser ablation of bulk gold in water in phase-explosion regime was compared for different laser pulsewidths in the broad range of 300 fs–100 ns, comparing a number of key ablation characteristics: mass loss, single-shot crater depth, and optical density of the generated colloidal solutions in the spectral ranges of interband transitions and localized plasmon resonance. Comparing to related air-based ablation results, at the given fluences such wet ablation resulted in the maximum ablation yield for the picosecond laser pulses, occurring at subcritical peak pulse powers to avoid laser-beam self-focusing. This effect was demonstrated to yield in incomplete, weaker and "fractional" focusing in the water filaments of laser pulses with supercritical peak powers, thus resulting in less intense ablation and NP generation. At the other, nanosecond-pulse extreme the low ablation yield was related to strong ablation plasma screening, providing mass removal according to the well-established scaling relationships for plasma. Illustrative comparison of the ablation and nanoparticle generation efficiency versus the broad femto-pico-nanosecond laser pulsewidth range was enabled, using the proposed extinction volume, colloidal ablated mass, colloidal ablation efficiency as novel universal quantitative productivity and ergonomicity criteria, for potential upscaling of laser production of nanoparticles in liquids.

Acknowledgment

Project supported by the Ministry of Science and Higher Education of the Russian Federation (Project No. 075-15-2020-775).

References

[1] Sajti C L, Sattari R, Chichkov B N and Barcikowski S 2010 *J. Phys. Chem. C* **114**
[2] Gökce B, Streubel R and Barcikowski S 2016 *Opt. Lett.* **41** 1486
[3] Ionin A, Ivanova A, Khmel'nitskii R, Klevkov Y, Kudryashov S, Mel'nik N, Nastulyavichus A, Rudenko A, Saraeva I, Smirnov N, Zayarny D, Baranov A, Kirilenko D, Brunkov P and Shakhmin A 2018 *Appl. Surf. Sci.* **436** 662
[4] Shi Y, Jiang Z, Cao J and Ehmann K F 2020 *Appl. Surf. Sci.* **500** 144286
[5] Smirnov N A, Kudryashov S I, Rudenko A A, Zayarny D A and Ionin A A 2021 *Appl. Surf. Sci.* **562** 150243
[6] Kudryashov S I, Nastulyavichus A A, Saraeva I N, Rudenko A A, Zayarny D A and Ionin A A 2020 *Appl. Surf. Sci.* **519** 146204
[7] Arakelyan S M, Veiko V P, Kutrovskaya S V, Kucherik A O, Osipov A V, Vartanyan T A and Itina T E 2016 *J. Nanoparticle Res.* **18** 155
[8] Dittrich S, Streubel R, McDonnell C, Huber H P, Barcikowski S and Gökce B 2019 *Appl. Phys. A* **125** 1
[9] Zhang D, GÖkce B and Barcikowski S 2017 *Chem. Rev.* **117** 3990
[10] Scaramuzza S, Zerbetto M and Amendola V 2016 *J. Phys. Chem. C* **120** 9453
[11] Tarasenka N, Nominé A, Nevar A, Nedelko M, Kabbara H, Bruyère S, Ghanbaja J, Noel C, Krasilin A, Zograf G, Milichko V, Kulachenkov N, Makarov S, Belmonte T and Tarasenko N 2020 *Phys. Rev. Appl.* **13** 014021
[12] Gentile L, Mateos H, Mallardi A, Dell'Aglio M, De Giacomo A, Cioffi N and Palazzo G 2021 *J. Nanoparticle Res.* **23** 1
[13] Sukhov I A, Simakin A V, Shafeev G A, Viau G and Garcia C 2012 *Quantum Electron.* **42** 453
[14] Starinskiy S V, Shukhov Y G and Bulgakov A V 2017 *Appl. Surf. Sci.* **396** 1765
[15] Goncharova D A, Kharlamova T S, Reutova O and Svetlichnyi V A 2021 *Colloids Surfaces A Physicochem. Eng. Asp.* **613** 126115
[16] Kudryashov S I, Samokhvalov A A, Nastulyavichus A A, Saraeva I N, Mikhailovskii V Y, Ionin A A and Veiko V P 2019 *Mater.* **12** 562
[17] Kabashin A V. and Meunier M 2003 *J. Appl. Phys.* **94** 7941
[18] Tarasenka N, Shustava E, Butsen A, Kuchmizhak A A, Pashayan S, Kulinich S A and Tarasenko N 2021 *Appl. Surf. Sci.* **554** 149570
[19] Pang B, Ma Y, Tian Z, Liu J, Wu S, Teng D, Li P and Liang C 2021 *J. Colloid Interface Sci.* **585** 452

[20] Tangeysh B, Tibbetts K M, Odhner J H, Wayland B B and Levis R J 2013 *J. Phys. Chem. C* **117** 18719

[21] Cheng-Yu Shih, René Streubel, Johannes Heberle, *et al.* 2018 *Nanoscale* **10** 6900

[22] Saraeva I N, Nastulyavichus A A, Kudryashov S I, Rudenko A A, Zayarny D A, Ionin A A, Klevkov Y V, Zhilnikova M I and Simakin A V 2019 *Laser Phys. Lett.* **16** 066004

[23] Saraeva I N, Kudryashov S I, Rudenko A A, Zhilnikova M I, Ivanov D S, Zayarny D A, Simakin A V, Ionin A A and Garcia M E 2019 *Appl. Surf. Sci.* **470** 1018

[24] Nastulyavichus A A, Kudryashov S I, Rudenko A A, Zayarny D A and Ionin A A 2020 *J. Phys. Conf. Ser.* **1692** 012010

[25] Streubel R, Bendt G and Gökce B 2016 *Nanotechnology* **27** 205602

[26] Menéndez-Manjón A, Wagener P and Barcikowski S 2011 *J. Phys. Chem. C* **115** 5108

[27] Maciulevičius M, Vinčiunas A, Brikas M, Butsen A, Tarasenka N, Tarasenko N and Račiukaitis G 2013 *Appl. Phys. A: Mater. Sci. Process.* **111** 289

[28] Kohsakowski S, Gökce B, Tanabe R, Wagener P, Plech A, Ito Y and Barcikowski S 2016 *Phys. Chem. Chem. Phys.* **18** 16585

[29] Streubel R, Barcikowski S, letters B G O and 2016 *osapublishing.org*

[30] Barcikowski S, Me/'nndez-Manjón A, Chichkov B, Brikas M and Račiukaitis G 2007 *Appl. Phys. Lett.* **91** 083113

[31] Sylvestre J P, Kabashin A V, Sacher E and Meunier M 2005 *Appl. Phys. A* **80** 753

[32] Kudryashov S I, Samokhvalov A A, Ageev E I, Petrov A A and Veiko V P 2018 *Int. J. Heat Mass Transfer* **127** 1095

[33] Danilov P A, Ionin A A, Kudryashov S I, Rudenko A A, Smirnov N A, Porfirev A P, Kuchmizhak A A, Vitrik O B, Kovalev M S and Krasin G K 2020 *Opt. Mater. Express* **10** 2717

[34] Smirnov N A, Kudryashov S I, Danilov P A, Nastulyavichus A A, Rudenko A A, Ionin A A, Kuchmizhak A A and Vitrik O B 2020 *Opt. Quantum Electron.* **52** 1

[35] Doñate-Buendía C, Mínguez-Vega G, Lancis J and Fernández-Alonso M 2019 *Photonics Res.* **7** 1249

[36] Kudryashov S I, Nguyen L V, Kirilenko D A, Brunkov P N, Rudenko A A, Busleev N I, Shakhmin A L, Semencha A V, Khmelnitsky R A, Melnik N N, Saraeva I N, Nastulyavichus A A, Ionin A A, Tolordava E R and Romanova Y M 2018 *ACS Appl. Nano Mater.* **1** 2461

[37] Lam J, Lombard J, Dujardin C, Ledoux G, Merabia S and Amans D 2016 *Appl. Phys. Lett.* **108** 074104

[38] Ibrahimkutty S, Wagener P, Menzel A, Plech A and Barcikowski S 2012 *Appl. Phys. Lett.* **101** 103104

[39] Ionin A A, Kudryashov S I and Seleznev L V 2010 *Phys. Rev. E* **82** 016404

[40] Jr C R P, Turner T P, Harrison R F, York G W, Osborne W Z, Anderson G K, Corlis X F, Haynes L C, Steele H S, Spicochi K C and King T R 1998 *J. Appl. Phys.* **64** 1083

[41] Gregg D W and Thomas S J *J. Appl. Phys.* **37** 2787

[42] Caruso A, Bertotti B and Giupponi P 1966 *Nuovo Cim. B* **45** 176

[43] Nemchinov I 1967 *J. Appl. Math. Mech.* **31** 320

[44] Basov N, Gribkov V, Krokhin O and Sklizkov G 1968 *Sov. Phys. JETP* **27** 575

[45] Nastulyavichus A A, Kudryashov S I, Smirnov N A, Rudenko A A, Kharin A Y, Zayarny D A bertovich and Ionin A A 2019 *Opt. Laser Technol.* **111** 75

[46] Kudryashov S I, Nastulyavichus A A, Ivanova A K, Smirnov N A, Khmelnitskiy R A, Rudenko A A, Saraeva I N, Tolordava E R, Yu. Kharin A, Zavestovskaya I N, Romanova Y M, Zayarny D A and Ionin A A 2019 *Appl. Surf. Sci.* **470** 825

[47] Yoo J H, Jeong S H, Greif R and Russo R E 2000 *J. Appl. Phys.* **88** 1638

[48] Yoo J H, Jeong S H, Mao X L, Greif R and Russo R E 2000 *Appl. Phys. Lett.* **76** 783

[49] Paul S, Kudryashov S I, Lyon K and Allen S D 2007 *Appl. Phys.* **101** 043106

[50] Kudryashov S I, Paul S, Lyon K and Allen S D 2011 *Appl. Phys. Lett.* **98** 254102

[51] Bulgakova N M, Evtushenko A B, Shukhov Y G, Kudryashov S I and Bulgakov A V 2011 *Appl. Surf. Sci.* **257** 10876

[52] Kudryashov S I, Tikhov A A and Zvorykin V D 2010 *Appl. Phys. A* **102** 493

[53] Neuenschwander B, Jaeggi B, Schmid M and Hennig G 2014 *Phys. Procedia* **56** 1047

[54] Smirnov N A, Kudryashov S I, Danilov P A, Rudenko A A, Ionin A A and Nastulyavichus A A 2018 *JETP Lett.* **108** 368

[55] Boyd R W, Shi Z and De Leon I 2014 *Opt. Commun.* **326** 74

[56] Smirnov N A, Kudryashov S I, Danilov P A, Rudenko A A, Gakovic B, Milovanović D, Ionin A A, Nastulyavichus A A and Umanskaya S F 2019 *Laser Phys. Lett.* **16** 056002

[57] Anisimov S I, Zhakhovsky V V, Inogamov N A, Migdal K P, Petrov Y V and Khokhlov V A 2019 *J. Exp. Theor. Phys.* **129** 757

[58] Petrov Y V, Inogamov N A, Anisimov S I, Migdal K P, Khokhlov V A and Khishchenko K V 2015 *J. Phys. Conf. Ser.* **653** 012087

[59] Ionin A A, Kudryashov S I, Makarov S V, Rudenko A A, Saltuganov P N, Seleznev L V, Sinitsyn D V and Sunchugasheva E S 2014 *Appl. Surf. Sci.* **292** 678

[60] Shih C Y, Shugaev M V, Wu C and Zhigilei L V 2020 *Phys. Chem. Chem. Phys.* **22** 7077

[61] Inogamov N A, Khokhlov V A, Petrov Y V and Zhakhovsky V V 2020 *Mol.* **25** 67

[62] Inogamov N A, Khokhlov V A, Petrov Y V and Zhakhovsky V V 2020 *Opt. Quantum Electron.* **52** 1

[63] Petrov Y V, Khokhlov V A, Zhakhovsky V V and Inogamov N A 2019 *Appl. Surf. Sci.* **492** 285

[64] Leveugle E, Ivanov D S and Zhigilei L V 2004 *Appl. Phys. A* **79** 1643

[65] Artyukov I A, Zayarniy D A, Ionin A A, Kudryashov S I, Makarov S V and Saltuganov P N 2014 *JETP Lett.* **99** 51

[66] Yang J, Zhao Y, Zhang N, Liang Y and Wang M 2007 *Phys. Rev. B* **76** 165430

[67] Wagener P, Schwenke A, Chichkov B N and Barcikowski S 2010 *J. Phys. Chem. C* **114** 7618

[68] Palik E D 2012 *Handbook of optical constants of solids Handb. Opt. Constants Solids* **1** 1

[69] Kohsakowski S, Santagata A, Dell'Aglio M, de Giacomo A, Barcikowski S, Wagener P and Gökce B 2017 *Appl. Surf. Sci.* **403** 487

[70] Shih C Y, Chen C, Rehbock C, Tymoczko A, Wiedwald U, Kamp M, Schuermann U, Kienle L, Barcikowski S and Zhigilei L V 2021 *J. Phys. Chem. C* **125** 2132

[71] Kudryashov S I 1999 "Thermodynamic characteristics of metastable liquid-vapor equilibrium of carbon at laser vaporization of polycrystalline graphite", Ph. D. Dissertation (Moscow State University)

[72] Viktor Myroshnychenko, Jessica Rodríguez-Fernández, Isabel Pastoriza-Santos, Funston A M, Carolina Novo, Paul Mulvaney, Liz-Marzán L M and de Abajo F J G 2008 *Chem. Soc. Rev.* **37** 1792

[73] Couairon A and Mysyrowicz A 2007 *Phys. Rep.* **441** 47

[74] Geints Y É, Zemlyanov A A, Ionin A A, Kudryashov S I, Seleznev L V, Sinitsyn D V and Sunchugasheva E S 2010 *J. Exp. Theor. Phys.* **111** 724

[75] Kiran P P, Bagchi S, Krishnan S R, Arnold C L, Kumar G R and Couairon A 2010 *Phys. Rev. A* **82** 013805

[76] Johnson A, Durfee C G, Adams D E, Kleinfeld D, Vitek D N, Squier J A, Tsai P S and Backus S 2010 *Opt. Express.* **18** 18086

[77] He F, Xu H, Xiong H, Ni J, Midorikawa K, Sugioka K, Cheng Y and Xu Z 2010 *Opt. Lett.* **35** 1106

[78] Xu C, Zhu G and Durst M E 2006 *Opt. Express.* **14** 12243

[79] Xu C, Zhu G, Howe J van, Durst M and Zipfel W 2005 *Opt. Express.* **13** 2153

[80] Durfee C G, Adams D E, Kleinfeld D, Vitek D N, Block E, Squier J A, Backus S and Bellouard Y 2010 *Opt. Express.* **18** 24673

[81] Kammel R, Ackermann R, Thomas J, Götte J, Skupin S, Tünnermann A and Nolte S 2014 *Light Sci. Appl.* **3** e169

[82] Kudryashov S, Danilov P, Schneider L, Schille J, Loeschner U, Nastulyavichus A, Smirnov N, Kuchmizhak A and Vitrik O 2021 *Laser Phys. Lett.* **18** 016101

[83] Waag F, Streubel R, Gökce B and Barcikowski S 2021 *Appl. Nanosci.* **11** 1303

[84] Jendrzej S, Gökce B, Epple M and Barcikowski S 2017 *ChemPhysChem* **18** 1012